#### **MATERIALS SCIENCE**

# Freestanding epitaxial SrTiO<sub>3</sub> nanomembranes via remote epitaxy using hybrid molecular beam epitaxy

Hyojin Yoon<sup>1+</sup>, Tristan K. Truttmann<sup>1+</sup>, Fengdeng Liu<sup>1</sup>, Bethany E. Matthews<sup>2</sup>, Sooho Choo<sup>1</sup>, Qun Su<sup>3</sup>, Vivek Saraswat<sup>4</sup>, Sebastian Manzo<sup>4</sup>, Michael S. Arnold<sup>4</sup>, Mark E. Bowden<sup>5</sup>, Jason K. Kawasaki<sup>4</sup>, Steven J. Koester<sup>3</sup>, Steven R. Spurgeon<sup>2,6</sup>, Scott A. Chambers<sup>7</sup>, Bharat Jalan<sup>1\*</sup>

The epitaxial growth of functional oxides using a substrate with a graphene layer is a highly desirable method for improving structural quality and obtaining freestanding epitaxial nanomembranes for scientific study, applications, and economical reuse of substrates. However, the aggressive oxidizing conditions typically used in growing epitaxial oxides can damage graphene. Here, we demonstrate the successful use of hybrid molecular beam epitaxy for SrTiO<sub>3</sub> growth that does not require an independent oxygen source, thus avoiding graphene damage. This approach produces epitaxial films with self-regulating cation stoichiometry. Furthermore, the film (46-nm-thick SrTiO<sub>3</sub>) can be exfoliated and transferred to foreign substrates. These results open the door to future studies of previously unattainable freestanding oxide nanomembranes grown in an adsorption-controlled manner by hybrid molecular beam epitaxy. This approach has potentially important implications for the commercial application of perovskite oxides in flexible electronics and as a dielectric in van der Waals thin-film electronics.

Copyright © 2022
The Authors, some rights reserved; exclusive licensee
American Association for the Advancement of Science. No claim to original U.S. Government Works. Distributed under a Creative
Commons Attribution
NonCommercial
License 4.0 (CC BY-NC).

#### INTRODUCTION

In conventional epitaxial growth, the epilayer is intimately linked to the substrate. This reality prevents the reuse of the expensive single-crystal substrate unless the film is to be sacrificed by polishing it away. Furthermore, permanently joining the film and substrate can generate challenges in characterizing a film due to signals from the substrate that are often many orders of magnitude stronger than those of the film (1). Therefore, there is both an economic and scientific impetus to develop facile methods of producing freestanding single-crystal nanomembranes (2).

The most rudimentary route is grinding (3) or etching (4) bulk wafers down to microscopic thicknesses, but this approach lacks precision and achieves poor material utilization because a majority of the wafer is sacrificed. A more precise technique uses a sacrificial layer between the substrate and film, which, upon removal, releases the thin film as a freestanding membrane. The sacrificial layer may be selectively melted (5) or etched (6, 7) away. In systems where the target film preferentially absorbs light, the film region adjacent to the transparent substrate can be selectively vaporized with intense laser light, thus becoming the sacrificial layer (8–11). Using a sacrificial layer offers the advantage of optionally reusing expensive substrates and has all the precision of the used thin-film growth technique. This approach has enabled studies that are possible only with freestanding membranes, including straining thin films

beyond levels possible with conventional biaxial strain (12) and the creation of Moiré twist heterostructures (13).

Another strategy for achieving freestanding single-crystalline membranes is to use an interface with weak adhesion, such as using one or more van der Waals materials (14). The technique takes on different names depending on the crystalline orientation. When the film is oriented to the van der Waals material, it is called van der Waals epitaxy (15, 16). If the film is oriented to the underlying substrate, the technique is called remote epitaxy (17). It is argued that the film nucleates on top of the van der Waals material and is oriented by the interatomic potential from the substrate penetrating through the van der Waals material. However, the underlying mechanism is still under debate because of the possibility of epitaxial lateral overgrowth through micro/nano holes in the van der Waals material (18). In practice, distinguishing these two mechanisms is challenging and has been a topic of substantial current interest. However, there is no doubt that the use of a van der Waals material is nonetheless a proven method to obtain freestanding single-crystalline membranes (14, 17) that has the advantages of high material utilization (no sacrificial layer required), optional substrate reuse (19), and the ability to obtain thin films with better crystal quality than in traditional epitaxy (20, 21).

Given the chemical flexibility and functional diversity of the perovskite oxide material family, extension of remote epitaxy to perovskite oxides is highly desirable as a method to potentially improve structural quality and to study freestanding membranes. Oxide molecular beam epitaxy (MBE) is a highly modular and adaptable lowenergy deposition technique that has been used to grow a wide range of perovskite oxides (22, 23). Conventional oxide MBE uses effusion cells to sublime or evaporate metals, and, more recently, metal suboxides (24), in conjunction with an oxygen source to oxidize the metals at the growth front, as shown in Fig. 1A. The oxygen source is often activated with an inductively coupled radio frequency (25, 26) or electron cyclotron resonance microwave (27) plasma, or it may be dilute or distilled ozone (28). Because these

<sup>&</sup>lt;sup>1</sup>Department of Chemical Engineering and Materials Science, University of Minnesota, Twin Cities, Minneapolis, MN 55455, USA. <sup>2</sup>Energy and Environment Directorate, Pacific Northwest National Laboratory, Richland, WA 99352, USA. <sup>3</sup>Department of Electrical and Computer Engineering, University of Minnesota, Twin Cities, Minneapolis, MN 55455, USA. <sup>4</sup>Department of Materials Science and Engineering, University of Wisconsin–Madison, Madison, WI 53706, USA. <sup>5</sup>Environmental Molecular Sciences Laboratory, Pacific Northwest National Laboratory, Richland, WA 99352, USA. <sup>6</sup>Pepartment of Physics, University of Washington, Seattle, WA 98195, USA. <sup>7</sup>Physical and Computational Sciences Directorate, Pacific Northwest National Laboratory, Richland, WA 99352, USA.

<sup>†</sup>These authors contributed equally to this work.

<sup>\*</sup>Corresponding author. Email: bjalan@umn.edu

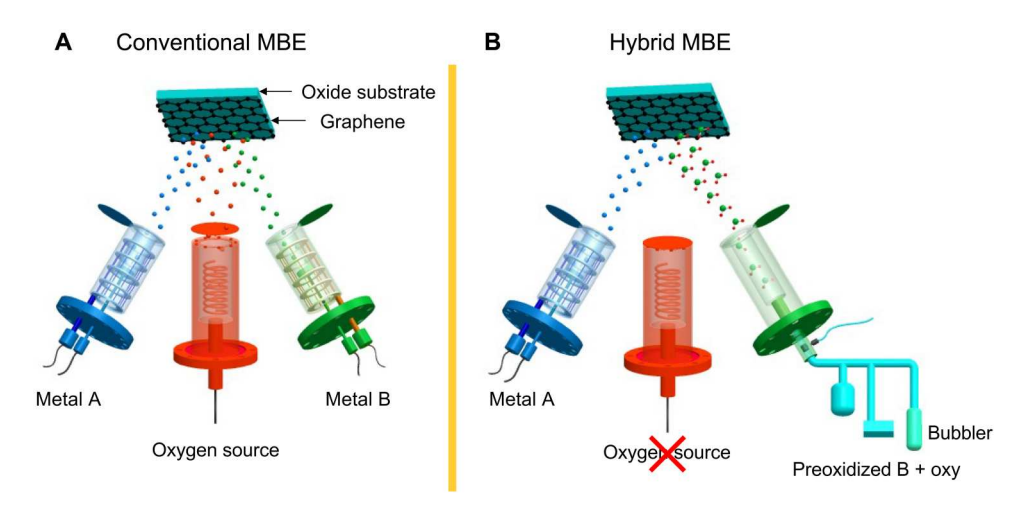


Fig. 1. Comparison of growth techniques for perovskite oxides on graphene. (A) Conventional oxide MBE. (B) Hybrid MBE modified by excluding oxygen. The gentle oxidation environment avoids graphene damage.

aggressive oxygen sources can decompose graphene, molecular oxygen supplied at a low background pressure of  $7 \times 10^{-7}$  torr has been used as a gentler source for remote epitaxy of oxides (29). However, it has not been possible to grow nanomembranes of complex oxides with self-regulating stoichiometry. For instance, SrTiO<sub>3</sub> films grown using conventional MBE (without an adsorption-controlled growth) would require precise flux control, which is typically no better than 0.1%, potentially resulting in a defect density as high as  $10^{19}~\rm cm^{-3}$  (23).

Hybrid MBE is a technique that addresses these problems by replacing the elemental Ti with a titanium tetraisopropoxide (TTIP) metal-organic source. The high vapor pressure of TTIP or its decomposition intermediates provides a desorption mechanism that self-regulates the Sr:Ti cation stoichiometry and provides a growth window within which the incorporated Sr:Ti ratio is unity and is impervious to flux instabilities (23, 30). The use of this technique has resulted in mobilities in SrTiO $_3$  films exceeding 120,000 cm $^2\mathrm{V}^{-1}\,\mathrm{s}^{-1}$  (31) using uniaxial strain, suggesting exciting opportunities for tunable electronic properties using membrane engineering.

In this study, we used hybrid MBE with the oxygen source turned off to avoid graphene damage, as shown in Fig. 1B. The four oxygen atoms in each TTIP molecule provide sufficient oxygen to obtain phase-pure  $SrTiO_3$ . We show that even without the use of additional oxygen, an adsorption-controlled growth is achievable, a key feature leading to hybrid MBE's high material quality. Critical to remote epitaxy, this aspect of hybrid MBE avoids graphene oxidation while allowing exfoliation and transfer of the epilayer to remote substrates. In contrast to prior reports of oxide remote epitaxy using dry-transfer graphene (17, 32), our approach yielded epitaxial  $SrTiO_3$  films on wet-transferred graphene (see figs. S1 and S2).

#### **RESULTS AND DISCUSSION**

Figure 2 shows the results of applying this technique to homoepitaxial  $SrTiO_3$  (without graphene). The clear reflection high-energy electron diffraction (RHEED) oscillations (Fig. 2B) and atomically smooth surfaces visible from atomic force microscopy (AFM; Fig. 2C, inset) show that this technique results in atomic precision even without the use of an independent oxygen source. Through high-resolution X-ray diffraction (HRXRD), a lattice parameter that is indistinguishable from the substrate (Fig. 2C) and a wide MBE growth window (Fig. 2D) indicate that this modified

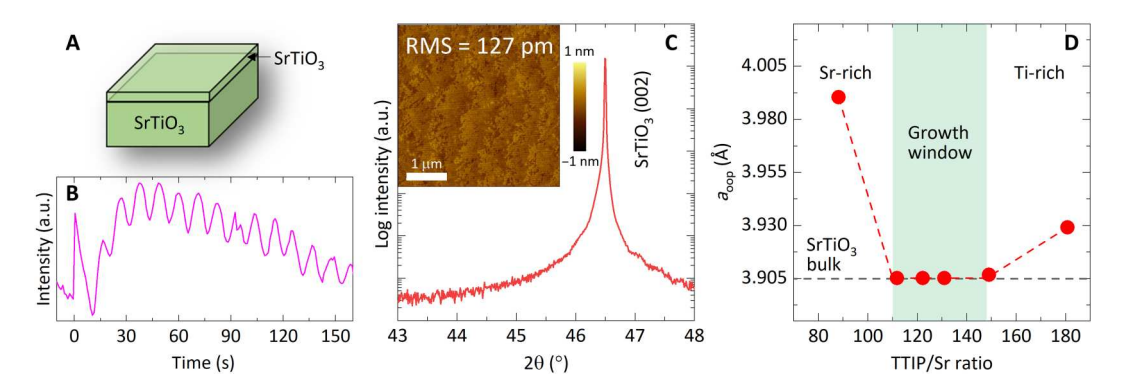


Fig. 2. Hybrid MBE of  $SrTiO_3$  without oxygen. (A) Schematic of the grown film structure  $SrTiO_3/SrTiO_3(001)$ . a.u., arbitrary units. (B) Intensity of RHEED spots versus time during growth. (C) HRXRD  $2\theta$ - $\omega$ -coupled scans and AFM (inset) of the resulting film. (D) The lattice parameter as a function of TTIP:Sr beam equivalent pressure (BEP) ratio during growth showing the presence of a MBE growth window.

technique also achieves adsorption-controlled growth with excellent structural quality and reproducibility.

Figure 3 shows results from the growth of SrTiO<sub>3</sub> on bare SrTiO<sub>3</sub> substrates (Fig. 3A) and on SrTiO<sub>3</sub> substrates covered with monolayer graphene (Fig. 3B), bilayer graphene (Fig. 3C), and on LSAT  $[(La_{0.18}Sr_{0.82})(Al_{0.59}Ta_{0.41})O_3]$  substrates covered with monolayer graphene (Fig. 3D). The RHEED patterns for films grown on bare substrates and on monolayer graphene show half-order streaks and Kikuchi lines characteristic of high-quality epitaxial SrTiO<sub>3</sub>, but the RHEED pattern on bilayer graphene is distinct. We later show, using scanning transmission electron microscopy (STEM), that the ring-like pattern in RHEED images may likely be associated with the in-plane rotation of SrTiO<sub>3</sub> film owing to poor graphene quality underneath. We also observed visible cracks in the sample with the monolayer graphene after SrTiO<sub>3</sub> growth, whereas no cracks were found in the bilayer graphene sample (fig. S3). Although the origin of these cracks is not well understood, we argue that their formation is associated with the poor quality of "wettransferred" graphene and the presence of polymethyl methacrylate (PMMA) residue.

These results, however, raise the question of whether the graphene remained intact or did it decompose during growth? Figure 4 (A and B) addresses this question with confocal Raman spectroscopy before and after growth of 46-nm SrTiO<sub>3</sub> on bilayer

graphene. Although the graphene D peak overlaps with a peak from SrTiO<sub>3</sub>, the similar positions and intensities of the graphene G and 2D peaks before and after growth indicate that the graphene remains intact and undamaged during growth. In addition, Fig. 4C shows that film exfoliation leaves behind graphene on the substrate. Further analysis using Raman mapping reveals that graphene remains present on the entire surface (fig. S4). This behavior should allow the substrate to be directly reused for growth of more epitaxial membranes. It is not clear why the SrTiO<sub>3</sub> film exfoliated at the film/graphene interface and not at the graphene/substrate interface. We argue that it is likely due to the difference in interfacial energy when graphene is placed on SrTiO<sub>3</sub> versus when SrTiO<sub>3</sub> is grown on graphene. Last, Fig. 4D shows that the film can be exfoliated and transferred to other substrates, as revealed by the presence of the SrTiO<sub>3</sub> (002) peak throughout the entire transfer process. The step-by-step description of the exfoliation/ transfer process is described in fig. S5. To investigate the structural quality of the film, we performed rocking curve scans of the SrTiO<sub>3</sub> (002) peak at each step of the transfer process and display the results in fig. S6. First, after SrTiO<sub>3</sub> growth on bilayer graphene, the rocking curve of the film and the substrate overlapped, yielding a narrow rocking curve [red line, full width at half maximum (FWHM) = 0.032°]. After exfoliation, the rocking curve became broad, which is likely due to the Kapton tape's microscopically

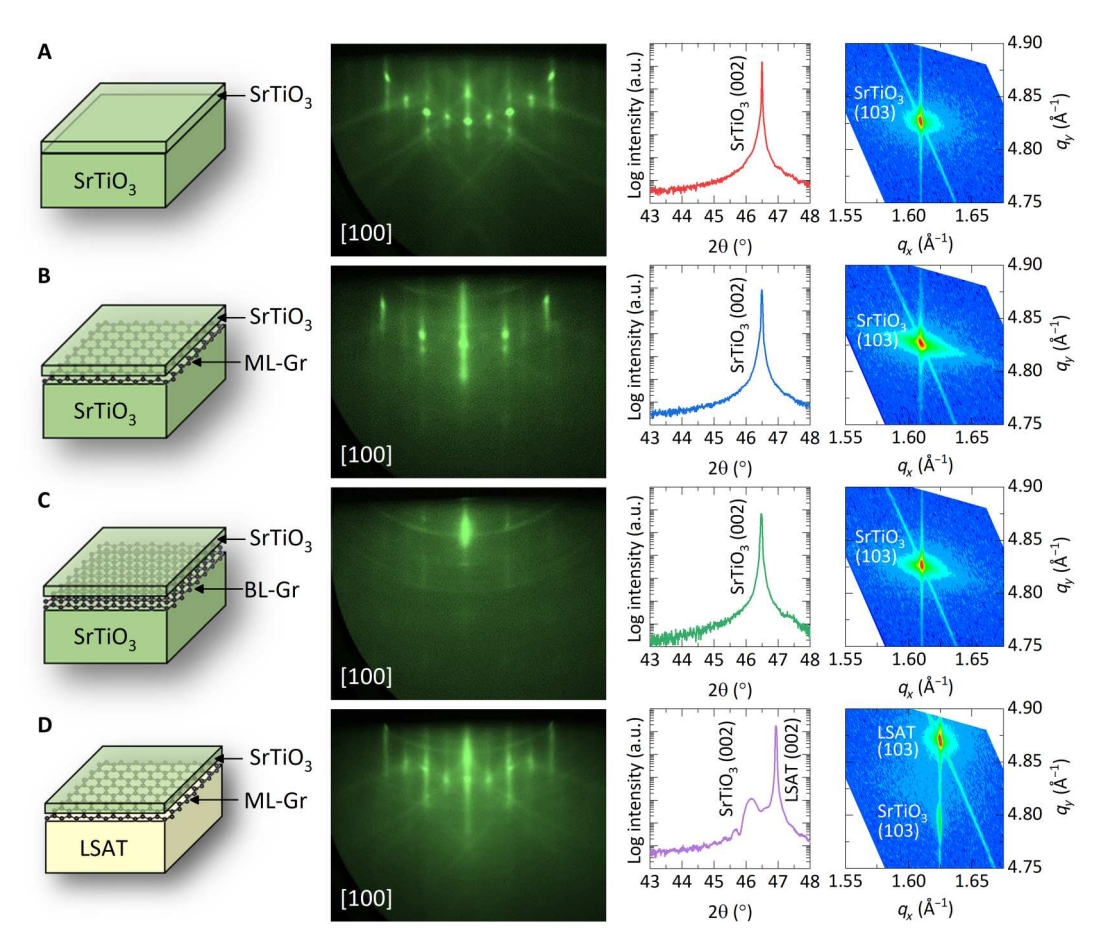
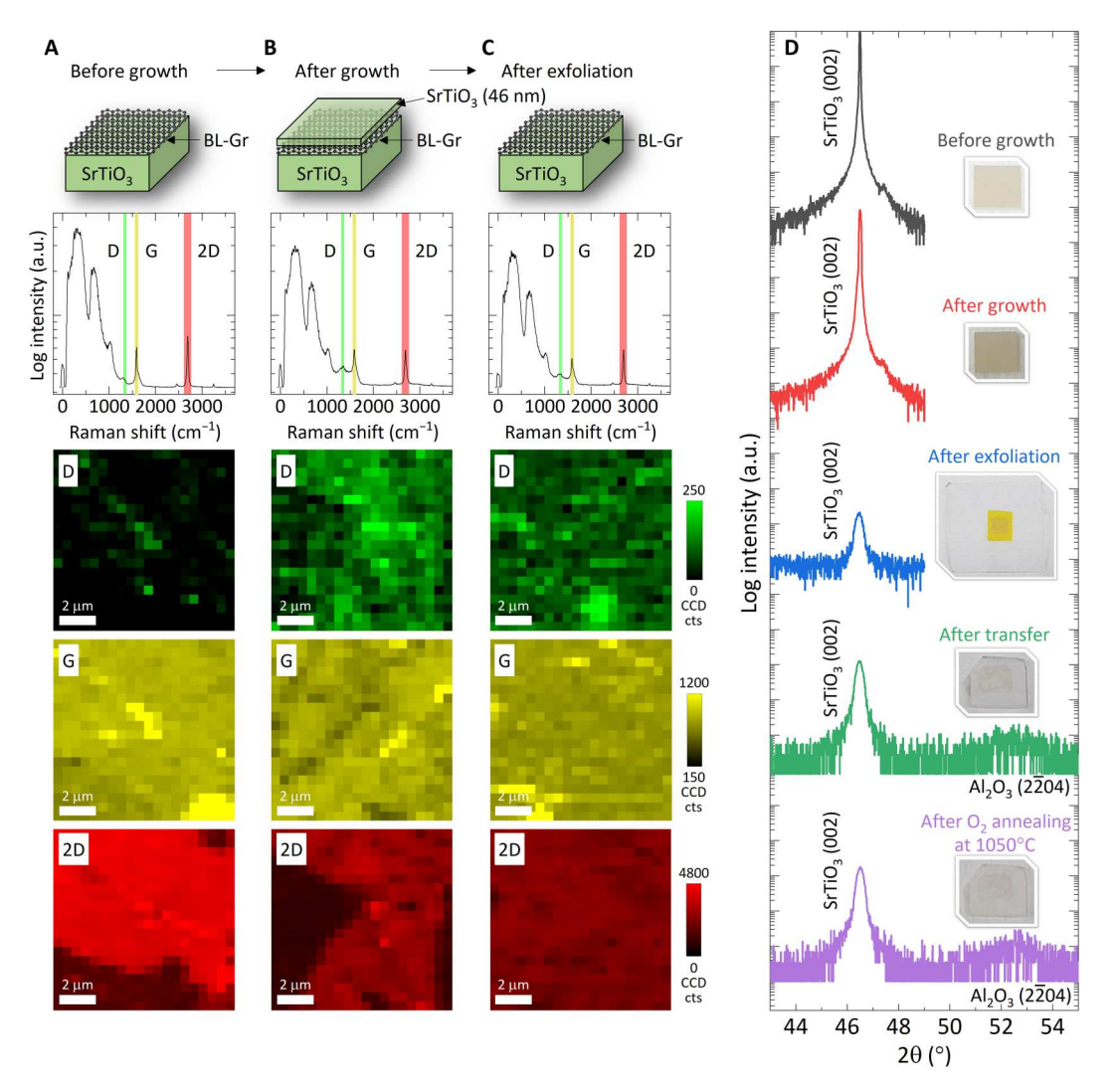


Fig. 3. Demonstration of epitaxy for perovskites on graphene using hybrid MBE. Sample schematic, RHEED, HRXRD  $2\theta$ - $\omega$ -coupled scans, and reciprocal space maps of (**A**) SrTiO<sub>3</sub>/SrTiO<sub>3</sub>(001), (**B**) SrTiO<sub>3</sub>/ML-Gr/SrTiO<sub>3</sub>(001), (**C**) SrTiO<sub>3</sub>/BL-Gr/SrTiO<sub>3</sub>(001), and (**D**) SrTiO<sub>3</sub>/ML-Gr/LSAT(001).



**Fig. 4. Demonstration of hybrid MBE-grown film exfoliation.** (**A** to **C**) Confocal Raman spectroscopy and microscopy of BL-Gr/SrTiO<sub>3</sub>(001) before growth (A), the resulting SrTiO<sub>3</sub>/BL-Gr/SrTiO<sub>3</sub>(001) after growth (B), and the restored BL-Gr/SrTiO<sub>3</sub>(001) via exfoliating the grown film (**C**). Each Raman micrograph shows the integrated intensity from one graphene peak scanned over the surface of the sample. (**D**) HRXRD  $2\theta$ -ω-coupled scans of the sample before growth and after growth, exfoliation, and then transfer to an r-plane Al<sub>2</sub>O<sub>3</sub> substrate.

rough surface (blue line, FWHM =  $2.388^\circ$ ). However, after transferring the exfoliated SrTiO $_3$  film onto the r-Al $_2$ O $_3$  substrate, the rocking curve became narrower again because of the atomically smooth surface of the r-Al $_2$ O $_3$  substrate (green line, FWHM =  $0.415^\circ$ ). We further annealed the SrTiO $_3$  film transferred onto the r-Al $_2$ O $_3$  substrate at  $1050^\circ$ C for 3 min under an excess of oxygen gas using rapid thermal annealing. Its rocking curve became only slightly narrower (purple line, FWHM =  $0.372^\circ$ ). These results show that the SrTiO $_3$  film grown on bilayer graphene had good crystalline quality rivaling that of the bulk SrTiO $_3$  substrate, and the increase in the rocking curve's FWHM after the exfoliation and transfer processes is likely due to defects resulting from exfoliation and transfer.

To directly image the structure, we performed STEM high-angle annular dark-field (STEM-HAADF) imaging and energy-dispersive X-ray spectroscopy (STEM-EDS) elemental mapping of the asgrown film before exfoliation and transfer. Consistent with the

above observations, the high-resolution STEM-HAADF image (fig. S7) further confirms cube-on-cube epitaxy. In Fig. 5, we show a large continuous region of epitaxial film containing a graphene defect. Specifically, we observe an in-plane rotation around the defect with an apparent [110] (001) // [100] (001) orientation relationship on one side of defect as shown in Figs. 5 (F and G), with the medium-angle annular dark-field (MAADF) and brightfield imaging in fig. S8. We find that three to four layers of graphene are preserved, with an approximate ~3.8 Å interlayer spacing. This graphene defect is likely the residual PMMA that was left despite the cleaning process (the details of the cleaning process are presented in Materials and Methods) or graphene "bunched" into faceted piles. These defects are a well-known problem with wet-transferred graphene (33, 34). It is therefore conceivable that these piles perturb the film growth, leading to the formation of domain boundaries at the pile apex and associated in-plane lattice rotation, likely resulting from local strain variations. Figure S9 further shows that the

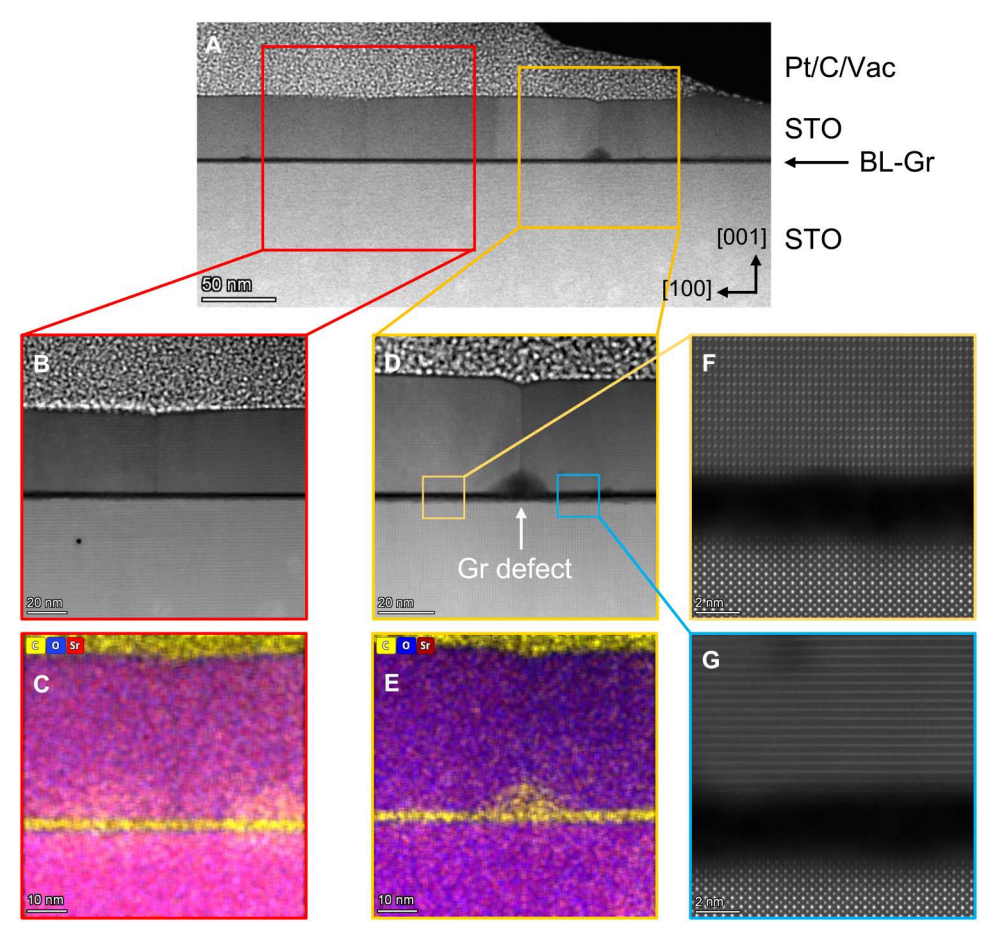


Fig. 5. STEM characterization of pretransfer SrTiO<sub>3</sub>. SrTiO<sub>3</sub> (STO)(**A**) Overview of a large film region containing pristine and defective graphene. STEM-HAADF images and STEM-EDS composition maps for the pristine (**B** and **C**) and defective (**D** and **E**) graphene regions, respectively. (**F** and **G**) STEM-HAADF images of the regions around the graphene defect, showing that the image in (F) shows a [110] (001) // [100] (001) epitaxial relationship, while the film in (G) is rotated slightly in-plane near the defect.

graphene thickness is largely uniform based on the method using the G/2D peak intensity ratio (35) and, therefore, is likely not responsible for in-plane rotation. As shown in Fig. 5 (F and G), carbon bunching results in large regions of ordered, on-zone domains interspersed with slightly rotated domains, which are nonetheless epitaxial out of plane. Together, these results attest to the compatibility of graphene with the hybrid MBE technique for complex oxide growth. A larger graphene thickness in STEM is likely due to graphene folding or oxidation during STEM specimen preparation, e.g., during the ion beam milling step.

Last, Fig. 6 shows STEM-HAADF and STEM-EDS composition maps of the transferred film after annealing (Fig. 4D, after O<sub>2</sub> annealing at 1050 °C). These data again reveal an epitaxial, single-phase film on the foreign substrate (r-Al<sub>2</sub>O<sub>3</sub>), confirming the successful transfer of an epitaxial SrTiO<sub>3</sub> film. This result is consistent with the X-ray diffraction data in Fig. 4D. Figure S10 shows wide-field-of-view STEM-HAADF images of films before and after transfer (A and B, respectively) showing defects similar to the partial square hole (void) visible in Fig. 6A. Because of the highly local nature of STEM analysis, the understanding of how prevalent these defects are in these films is limited; nonetheless, the linear density of defects appears much lower in the as-grown film (1 defect over 500 nm) than in the film after transfer (8 to 10 defects

over 500 nm). Consistent with the broadening of FWHM in rocking curve, these results suggest that the source of these defects is likely the exfoliation/transfer/annealing process.

In summary, we have demonstrated a novel hybrid MBE approach for growing epitaxial films of SrTiO<sub>3</sub> on graphene using Sr and TTIP sources without the use of an additional oxygen source. The technique produces films with atomic thickness control and self-regulated cation stoichiometry within a growth window. The films can be exfoliated as freestanding membranes and transferred to other substrates. This work opens the door to a wide range of studies on freestanding oxide membranes with the benefits afforded by hybrid MBE. Future studies will explore improving the quality of these films with dry-transferred or in-situgrown graphene and investigate a wider variety of material systems and heterostructures. However, the fact that the use of wet-transferred graphene also supports the epitaxial growth clearly suggests the robustness of remote epitaxy process adding to its versatile nature.

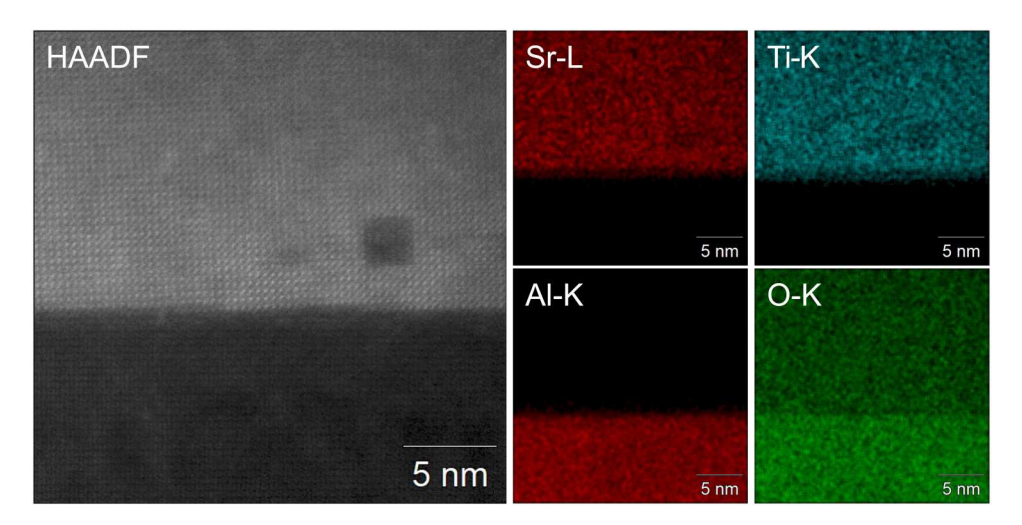


**Fig. 6. STEM characterization of transferred SrTiO<sub>3</sub> on r-Al<sub>2</sub>O<sub>3</sub>.** STEM of a SrTiO<sub>3</sub> epitaxial nanomembrane transferred to a foreign r-plane Al<sub>2</sub>O<sub>3</sub> substrate. The gray-scale image shows a STEM-HAADF image, whereas the colored images show the STEM-EDS elemental maps of the same region. The dark square region indicates a potential void in the film. Lattice vectors are given relative to the  $R\overline{3}c$  (r-Al<sub>2</sub>O<sub>3</sub>) and  $Pm\overline{3}m$  (STO) space groups, respectively.

#### **MATERIALS AND METHODS**

#### Graphene growth and transfer

Graphene was grown on both sides of polycrystalline copper foil using chemical vapor deposition in a quartz tube furnace. First, the foil was hydrogen-annealed in 16 standard cubic centimeters per minute (sccm) of hydrogen at 30 mTorr, while the furnace ramped to the growth temperature of 1050 °C (over ~20 min). Then, the foil was annealed for another 30 min at the growth temperature under the same flow and pressure. To grow graphene, 21-sccm hydrogen and 0.105-sccm methane were supplied while the furnace was maintained at 250 mTorr for 30 min. These conditions create self-terminating growth of one graphene monolayer. Then, the methane flow was stopped, and the hydrogen flow was set to 16 sccm while the furnace cooled off (~3 hours).

A solution of 4 weight percent PMMA with a molecular weight of 950,000 atomic mass units dissolved in chlorobenzene (PMMA 950 C4, MicroChem Corp.) was used for spin coating. Then, graphene was removed from the bottom side of the copper foil with a 10-s exposure to oxygen plasma in a reactive ion etcher. Ammonium persulfate solution [7 g of  $(NH_4)_2S_2O_8$  in 1 liter of deionized (DI) water] was used as a copper etchant to etch away the copper foil. Next, the remaining graphene was scooped and moved to the DI water for cleaning. Then, the cleaned graphene was scooped onto the target substrate using a flow mesh. After transferring the graphene to the substrate, it was baked for 15 min. The baked sample was submerged in acetone for 48 hours and rinsed in fresh acetone and isopropyl alcohol to remove the PMMA residue. The reader is referred to fig. S1 for a step-by-step guide of the graphene growth and transfer process.

#### SrTiO<sub>3</sub> epitaxial film growth

All films were grown using an oxide MBE (Scienta Omicron) on 5 mm–by–5 mm substrates of single-crystal SrTiO $_3$  (001) or LSAT (001) with and without a graphene layer. During growth, the substrates were maintained at a thermocouple reading of 900°C using a SiC-filament substrate heater. Strontium was supplied by thermal sublimation of distilled Sr dendrites (99.99% pure; Sigma-

Aldrich). Titanium and oxygen were supplied by the chemical precursor TTIP (99.999% pure; Sigma-Aldrich), which was fed to a line-of-sight gas injector (E-Science Inc.) via a custom gas inlet system using a linear leak valve and a Baratron capacitance manometer (MKS Instruments Inc.) in a feedback loop to control the TTIP flow entering the chamber. Immediately after the substrate temperature setpoint reached idle, the RHEED pattern was collected in the same chamber where growth took place. The reader is referred to fig. S5 for a step-by-step guide to the membrane exfoliation and transfer process.

#### Characterization

The sample surface topography was measured by a Bruker Nanoscope V Multimode 8 AFM in contact mode. All X-ray diffraction was performed with a Rigaku SmartLab XE diffractometer. Reciprocal space maps were collected with the HyPix-3000 detector in 1D mode to simultaneously resolve  $2\theta$  while  $\omega$  was scanned. Confocal Raman data were collected with a Witec Alpha 300 R confocal Raman microscope. The 532-nm source light was generated by a frequency-doubled Nd:yttrium-aluminum-garnet laser, and the output was analyzed with a diffraction grating spectrometer and a charge-coupled device detector.

Cross-sectional STEM samples were prepared using a FEI Helios NanoLab DualBeam Ga<sup>+</sup> Focused Ion Beam microscope with a standard lift-out procedure. STEM images were acquired on a probe-corrected Thermo Fisher Scientific Themis Z microscope operating at 300 kV, with a convergence semiangle of 25.2 mrad and an approximate collection angle range of 65 to 200 mrad, 16 to 62 mrad, and 8 to 14 mrad for STEM-HAADF, STEM-MAADF, and STEM low-angle annular dark-field, respectively. The STEM-EDS composition maps shown in Fig. 5 were acquired using a SuperX detector. The STEM-HAADF image shown in Fig. 6 was acquired on a probe-corrected JEOL GrandARM-300F microscope operating at 300 kV, with a convergence semiangle of 29.7 mrad and a collection angle range of 75 to 515 mrad. The STEM-EDS composition maps shown in Fig. 6 were acquired using a dual JEOL Centurio silicon drift detector setup.

#### **Supplementary Materials**

This PDF file includes:

Figs. S1 to S10

#### REFERENCES AND NOTES

- L. R. Thoutam, T. K. Truttmann, A. K. Rajapitamahuni, B. Jalan, Hysteretic magnetoresistance in a non-magnetic SrSnO<sub>3</sub> film via thermal coupling to dynamic substrate behavior. *Nano Lett.* 21, 10006–10011 (2021).
- F. M. Chiabrera, S. Yun, Y. Li, R. T. Dahm, H. Zhang, C. K. R. Kirchert, D. V. Christensen, F. Trier, T. S. Jespersen, N. Pryds, Freestanding perovskite oxide films: Synthesis, challenges, and properties. *Ann. Phys.* 534, 2200084 (2022).
- 3. J. N. Shive, The double-surface transistor. Phys. Rev. 75, 689-690 (1949).
- 4. W. E. Bradley. (U.S. Patent 2,846,346, 1954).
- 5. A. G. Milnes, D. L. Feucht. (U.S. Patent 4,159,354, 1976).
- 6. S. Deutscher, E. Grunbaum. (U.S. Patent 4,255,208, 1981).
- D. Lu, D. J. Baek, S. S. Hong, L. F. Kourkoutis, Y. Hikita, H. Y. Hwang, Synthesis of freestanding single-crystal perovskite films and heterostructures by etching of sacrificial water-soluble layers. *Nat. Mater.* 15, 1255–1260 (2016).
- W. S. Wong, T. Sands, N. W. Cheung, Damage-free separation of GaN thin films from sapphire substrates. Appl. Phys. Lett. 72, 599–601 (1998).
- L. Tsakalakos, T. Sands, Excimer laser liftoff of epitaxial Pb(Zr,Ti)O<sub>3</sub> thin films and heterostructures. MRS OPL 596. 549–556 (1999).
- G. J. Hayes, B. M. Clemens, Laser liftoff of gallium arsenide thin films. MRS Commun. 5, 1–5 (2015).
- A. Jan, B. A. Reeves, Y. van de Burgt, G. J. Hayes, B. M. Clemens, Threshold fluence measurement for laser liftoff of InP thin films by selective absorption. *Adv. Eng. Mater.* 20, 1700624 (2018).
- S. S. Hong, M. Gu, M. Verma, V. Harbola, Y. Wang Bai, D. Lu, A. Vailionis, Y. Hikita, R. Pentcheva, J. M. Rondinelli, H. Y. Hwang, Extreme tensile strain states in La<sub>0.7</sub>Ca<sub>0.3</sub>MnO<sub>3</sub> membranes. Science 368, 71–76 (2020).
- Y. Li, C. Xiang, F. M. Chiabrera, S. Yun, H. Zhang, D. J. Kelly, R. T. Dahm, C. K. R. Kirchert, T. E. L. Cozannet, F. Trier, D. V. Christensen, T. J. Booth, S. B. Simonsen, S. Kadkhodazadeh, T. S. Jespersen, N. Pryds, Stacking and twisting of freestanding complex oxide thin films. Adv. Mater. 34, 2203187 (2022).
- K. Chung, C.-H. Lee, G.-C. Yi, Transferable GaN layers grown on ZnO-coated graphene layers for optoelectronic devices. Science 330, 655–657 (2010).
- A. Koma, K. Sunouchi, T. Miyajima, Fabrication and characterization of heterostructures with subnanometer thickness. *Microelectron. Eng.* 2, 129–136 (1984).
- T. Löher, Y. Tomm, C. Pettenkofer, W. Jaegermann, Van der Waals epitaxy of three-dimensional CdS on the two-dimensional layered substrate MoTe<sub>2</sub>(0001). Appl. Phys. Lett. 65, 555–557 (1994).
- Y. Kim, S. S. Cruz, K. Lee, B. O. Alawode, C. Choi, Y. Song, J. M. Johnson, C. Heidelberger, W. Kong, S. Choi, K. Qiao, I. Almansouri, E. A. Fitzgerald, J. Kong, A. M. Kolpak, J. Hwang, J. Kim, Remote epitaxy through graphene enables two-dimensional material-based layer transfer. *Nature* 544, 340–343 (2017).
- S. Manzo, P. J. Strohbeen, Z. H. Lim, V. Saraswat, D. Du, S. Xu, N. Pokharel, L. J. Mawst, M. S. Arnold, J. K. Kawasaki, Pinhole-seeded lateral epitaxy and exfoliation of GaSb films on graphene-terminated surfaces. *Nat. Commun.* 13, 4014 (2022).
- J. Kim, C. Bayram, H. Park, C.-W. Cheng, C. Dimitrakopoulos, J. A. Ott, K. B. Reuter,
   W. Bedell, D. K. Sadana, Principle of direct van der Waals epitaxy of single-crystalline films on epitaxial graphene. *Nat. Commun.* 5, 4836 (2014).
- J. Jiang, X. Sun, X. Chen, B. Wang, Z. Chen, Y. Hu, Y. Guo, L. Zhang, Y. Ma, L. Gao, F. Zheng, L. Jin, M. Chen, Z. Ma, Y. Zhou, N. P. Padture, K. Beach, H. Terrones, Y. Shi, D. Gall, T.-M. Lu, E. Wertz, J. Feng, J. Shi, Carrier lifetime enhancement in halide perovskite via remote epitaxy. *Nat. Commun.* 10, 4145 (2019).
- T. Journot, H. Okuno, N. Mollard, A. Michon, R. Dagher, P. Gergaud, J. Dijon, A. V. Kolobov, B. Hyot, Remote epitaxy using graphene enables growth of stress-free GaN. *Nanotechnology* 30, 505603 (2019).
- D. G. Schlom, Perspective: Oxide molecular-beam epitaxy rocks! APL Mater. 3, 062403 (2015).
- W. Nunn, T. K. Truttmann, B. Jalan, A review of molecular-beam epitaxy of wide bandgap complex oxide semiconductors. J. Mater.Res 36, 4846–4864 (2021).
- K. M. Adkison, S.-L. Shang, B. J. Bocklund, D. Klimm, D. G. Schlom, Z.-K. Liu, Suitability of binary oxides for molecular-beam epitaxy source materials: A comprehensive thermodynamic analysis. APL Mater. 8, 081110 (2020).

- J.-P. Locquet, In situ MBE growth of epitaxial CuO films with a source of activated oxygen.
   J. Less Common Met. 164-165. 300–306 (1990).
- J. P. Locquet, E. M\u00e4chler, Characterization of a radio frequency plasma source for molecular beam epitaxial growth of high-T<sub>c</sub> superconductor films. J. Vac. Sci. Technol. A 10, 3100–3103 (1992).
- D. M. Lind, S. D. Berry, G. Chern, H. Mathias, L. R. Testardi, Growth and structural characterization of Fe<sub>3</sub>O<sub>4</sub> and NiO thin films and superlattices grown by oxygen-plasma-assisted molecular-beam epitaxy. *Phys. Rev. B* 45, 1838–1850 (1992).
- D. D. Berkley, B. R. Johnson, N. Anand, K. M. Beauchamp, L. E. Conroy, A. M. Goldman, J. Maps, K. Mauersberger, M. L. Mecartney, J. Morton, M. Tuominen, Y.-J. Zhang, In situ formation of superconducting YBa<sub>2</sub>Cu<sub>3</sub>O<sub>7-x</sub> thin films using pure ozone vapor oxidation.
   Appl. Phys. Lett. 53, 1973–1975 (1988).
- H. S. Kum, H. Lee, S. Kim, S. Lindemann, W. Kong, K. Qiao, P. Chen, J. Irwin, J. H. Lee, S. Xie,
   S. Subramanian, J. Shim, S.-H. Bae, C. Choi, L. Ranno, S. Seo, S. Lee, J. Bauer, H. Li, K. Lee,
   J. A. Robinson, C. A. Ross, D. G. Schlom, M. S. Rzchowski, C.-B. Eom, J. Kim, Heterogeneous integration of single-crystalline complex-oxide membranes. *Nature* 578, 75–81 (2020).
- B. Jalan, P. Moetakef, S. Stemmer, Molecular beam epitaxy of SrTiO<sub>3</sub> with a growth window. Appl. Phys. Lett. 95, 032906 (2009).
- J. Son, P. Moetakef, B. Jalan, O. Bierwagen, N. J. Wright, R. Engel-Herbert, S. Stemmer, Epitaxial SrTiO<sub>3</sub> films with electron mobilities exceeding 30,000 cm<sup>2</sup>V<sup>-1</sup>s<sup>-1</sup>. *Nat. Mater.* 9, 482–484 (2010).
- H. Kim, K. Lu, Y. Liu, H. S. Kum, K. S. Kim, K. Qiao, S.-H. Bae, S. Lee, Y. J. Ji, K. H. Kim, H. Paik, S. Xie, H. Shin, C. Choi, J. H. Lee, C. Dong, J. A. Robinson, J.-H. Lee, J.-H. Ahn, G. Y. Yeom, D. G. Schlom, J. Kim, Impact of 2D–3D heterointerface on remote epitaxial interaction through graphene. ACS Nano 15, 10587–10596 (2021).
- 33. Y.-C. Lin, C.-C. Lu, C.-H. Yeh, C. Jin, K. Suenaga, P.-W. Chiu, Graphene annealing: How clean can it be? *Nano Lett.* **12**, 414–419 (2012).
- W. S. Leong, H. Wang, J. Yeo, F. J. Martin-Martinez, A. Zubair, P.-C. Shen, Y. Mao, T. Palacios, M. J. Buehler, J.-Y. Hong, J. Kong, Paraffin-enabled graphene transfer. *Nat. Commun.* 10, 867 (2019).
- 35. V. Kumar, A. Kumar, D.-J. Lee, S.-S. Park, Estimation of number of graphene layers using different methods: A focused review. *Materials (Basel)* **14**, 4590 (2021).

Acknowledgments: We thank J. Kim for discussion. Funding: Hybrid MBE growth and characterization of SrTiO<sub>3</sub> films were supported by the U.S. Department of Energy (DOE) through grant DE-SC0020211. Graphene growth and integration with the oxide substrate was supported by the Air Force Office of Scientific Research through grants FA9550-21-0460 and FA9550-21-1-0025. Film growth was performed using instrumentation funded by DURIP award FA9550-18-1-0294. Preliminary graphene growth and sample preparation at the University of Wisconsin was supported by the DOE, Office of Science, Basic Energy Sciences, under award no. DE-SC0016007, and the NSF through grant DMR-1752797. Parts of this work were carried out at the Characterization Facility, University of Minnesota, which receives partial support from the NSF through the MRSEC program under award DMR-2011401. Substrate preparation was carried out at the Minnesota Nano Center, which is supported by the NSF through the National Nano Coordinated Infrastructure under award ECCS-2025124. STEM and XPS were supported by the DOE, Office of Science, Office of Basic Energy Sciences, Division of Materials Sciences and Engineering under award no. 10122, Pacific Northwest National Laboratory (PNNL) is a multiprogram national laboratory operated by Battelle for the DOE under contract DE-AC05-79RL01830. We acknowledge facility support from the Environmental Molecular Sciences Laboratory, a DOE Office of Science User Facility sponsored by the Biological and Environmental Research program and located at PNNL. A portion of the microscopy work was performed in the Radiological Microscopy Suite (RMS), located in the Radiochemical Processing Laboratory (RPL) at PNNL. Author contributions: H.Y., T.K.T., and B.J. conceived the idea and designed the experiments. H.Y. and T.K.T. developed the growth technique. H.Y. grew and transferred the graphene, grew the films, and transferred the films to foreign substrates. Q.S. performed the initial graphene transfer under the direction of S.J.K. S.M. transferred some of the graphene to foreign substrates under the supervision of J.K.K. H.Y., S.C., and F.L. characterized the films with AFM, HRXRD, and confocal Raman spectroscopy. H.Y. and S.C. curated the data under the supervision of B.J. B.E.M. performed STEM measurement and analysis under the supervision of S.R.S. and S.A.C. M.E.B. conducted additional XRD analysis. T.K.T., H.Y., and B.J. wrote the manuscript with input and feedback from all the authors. B.J. directed and organized the different aspects of the project. Competing interests: The authors declare that they have no competing interests. Data and materials availability: All data needed to evaluate the conclusions in the paper are present in the paper and/or the Supplementary Materials.

Submitted 17 June 2022 Accepted 8 November 2022 Published 23 December 2022 10.1126/sciadv.add5328

## **Science** Advances

### Freestanding epitaxial SrTiO<sub>3</sub> nanomembranes via remote epitaxy using hybrid molecular beam epitaxy

Hyojin Yoon, Tristan K. Truttmann, Fengdeng Liu, Bethany E. Matthews, Sooho Choo, Qun Su, Vivek Saraswat, Sebastian Manzo, Michael S. Arnold, Mark E. Bowden, Jason K. Kawasaki, Steven J. Koester, Steven R. Spurgeon, Scott A. Chambers, and Bharat Jalan

Sci. Adv., **8** (51), eadd5328. DOI: 10.1126/sciadv.add5328

View the article online

https://www.science.org/doi/10.1126/sciadv.add5328

**Permissions** 

https://www.science.org/help/reprints-and-permissions

Use of this article is subject to the Terms of service